RESEARCH ARTICLE

The temporal dynamics of chromosome instability in ovarian cancer cell lines and primary patient samples

Signe Penner-Goeke[1,2], Zelda Lichtensztejn[1,2], Megan Neufeld[1,2], Jennifer L. Ali[1], Alon D. Altman[3], Mark W. Nachtigal[1,2,3], Kirk J. McManus[1,2]*

1 Department of Biochemistry and Medical Genetics, University of Manitoba, Winnipeg, Manitoba, Canada, **2** Research Institute in Oncology and Hematology, CancerCare Manitoba, Winnipeg, Manitoba, Canada, **3** Department of Obstetrics, Gynecology and Reproductive Sciences, University of Manitoba, Winnipeg, Manitoba, Canada

* Kirk.McManus@umanitoba.ca

Abstract

Epithelial ovarian cancer (EOC) is the most prevalent form of ovarian cancer and has the highest mortality rate. Novel insight into EOC is required to minimize the morbidity and mortality rates caused by recurrent, drug resistant disease. Although numerous studies have evaluated genome instability in EOC, none have addressed the putative role chromosome instability (CIN) has in disease progression and drug resistance. CIN is defined as an increase in the rate at which whole chromosomes or large parts thereof are gained or lost, and can only be evaluated using approaches capable of characterizing genetic or chromosomal heterogeneity within populations of cells. Although CIN is associated with numerous cancer types, its prevalence and dynamics in EOC is unknown. In this study, we assessed CIN within serial samples collected from the ascites of five EOC patients, and in two well-established ovarian cancer cell models of drug resistance (PEO1/4 and A2780s/cp). We quantified and compared CIN (as measured by nuclear areas and CIN Score (CS) values) within and between serial samples to glean insight into the association and dynamics of CIN within EOC, with a particular focus on resistant and recurrent disease. Using quantitative, single cell analyses we determined that CIN is associated with every sample evaluated and further show that many EOC samples exhibit a large degree of nuclear size and CS value heterogeneity. We also show that CIN is dynamic and generally increases within resistant disease. Finally, we show that both drug resistance models (PEO1/4 and A2780s/cp) exhibit heterogeneity, albeit to a much lesser extent. Surprisingly, the two cell line models exhibit remarkably similar levels of CIN, as the nuclear areas and CS values are largely overlapping between the corresponding paired lines. Accordingly, these data suggest CIN may represent a novel biomarker capable of monitoring changes in EOC progression associated with drug resistance.

Author summary

Ovarian cancer is one of the most lethal cancers in women due to the high prevalence of
drug resistant disease. New insight into the biology causing drug resistance is required to
reduce death rates associated with the disease. In many cancer types, chromosome instability
(CIN; or abnormal numbers of chromosomes) is associated with aggressive tumours, the
acquisition of multi-drug resistance and poor patient outcome, yet CIN is poorly character-
ized in ovarian cancer. Here, we employ a new microscopy-based approach to examine the
presence and dynamics of CIN within single cells obtained from ovarian cancer patients col-
lected over time. We show that CIN is associated with every sample and further show that
increases in CIN are associated with treatment and/or the development of drug (platinum)
resistant disease. Although additional studies are required, these findings suggest CIN may
be a new biomarker that can monitor disease progression, particularly in response to ther-
apy. Finally, we demonstrate that CIN is low in two cellular models of drug resistant disease.
Collectively, our findings strengthen the need for studies employing patient-derived samples
to accurately assess the abnormal biology associated with the disease, and cautions the use of
these cell models in studies related to drug resistance that may arise from CIN.

Introduction

Novel insight into epithelial ovarian cancer (EOC) pathogenesis is essential to reduce the high
mortality rate caused by recurrent, drug-resistant disease. EOCs comprise the most frequent
type of ovarian cancer (incidence of 10.8 per 100 000 women in Canada) and have the highest
mortality rate (152 000 deaths worldwide in 2012)[1]. There are two histologic subgroups
where Type 1 includes mucinous, low grade serous, low/moderate grade endometrioid, and
clear cell cancers, and Type 2 includes moderate/high grade serous, high grade endometrioid,
undifferentiated, and malignant mixed mesodermal tumours[2]. Chemotherapy may be the
only viable treatment in EOC patients where the mass or spread of the tumours limits surgical
debulking. While many patients may respond initially to adjuvant chemotherapy (usually 6–9
cycles of cisplatin or carboplatin, plus a taxane), as much as 75% of patients will relapse within
18 months[3] with chemoresistant disease. Chemoresistant disease is defined as disease recur-
rence within 6 months of initial treatment. EOCs that reoccur are typically incurable; however,
response rates have been observed in 10–30% of patients treated with gemcitabine, liposomal
doxorubicin (Caelyx), or topotecan, which has increased their progression-free survival[4–6].
One of the fundamental priorities identified at the 2015 Ovarian Cancer Action meeting was
to characterize genome instability in acquired drug resistant disease[7]. We propose that a
more complete understanding of the molecular mechanisms driving genomic instability in
EOC is essential to enhance our prognostic, diagnostic, and therapeutic capabilities.

In general, chromosome instability (CIN) is one of several mechanisms suspected to drive
and promote genome instability[8–10]. CIN is defined as an increase in the rate at which
whole chromosomes or large parts thereof are gained or lost (see [11]). To accurately assess
CIN mandates the use of single cell approaches capable of characterizing genetic or chromo-
somal heterogeneity within a given population[11]. CIN typically manifests due to errors in
DNA replication, DNA repair or chromosome segregation (reviewed in [12, 13]), and is of par-
ticular interest as in many cancer types, CIN is associated with aggressive tumors, the acquisi-
tion of drug resistance and poor patient prognosis[14–19]. Numerous studies have evaluated
various aspects of genome instability in EOC, with a particular focus on the most prevalent
form of EOC, high-grade serous ovarian cancer (HGSOC)[20–29]. For example, HGSOC is

characterized by gene copy number variations, structural variants, single nucleotide variants, and sometimes highly rearranged genomes[23, 27, 30]. However, many of these studies employ DNA sequencing or single nucleotide polymorphisms (SNP) analyses to characterize this genome instability in DNA extracted from large numbers of cells (e.g. 10^3 to 10^6 cells)[20–29]. Thus, these results are heavily impacted by population averaging and are incapable of characterizing the karyotypic complexity and heterogeneity typically associated with CIN. Furthermore, because aneuploidy (*i.e.* abnormal chromosome numbers) is frequently used as a surrogate marker for CIN, traditional studies have also employed cytogenetic approaches including karyotypic analyses and comparative genomic hybridization (CGH) to assess aneuploidy or CIN within a given sample. While these approaches have identified karyotypic differences between samples, they typically only report a modal karyotype for any given sample, which is usually drawn from 25–30 mitotic chromosome spreads. Consequently, these approaches are limited in scope as they are costly, time consuming, limited in capacity, and incapable of adequately quantifying the cell-to-cell heterogeneity induced by CIN within hundreds of cells from a given sample, particularly over time.

To begin to address the limitations of conventional approaches and more accurately quantify the heterogeneous nature of CIN, we previously developed and validated two independent image-based approaches that evaluate surrogate markers of CIN, namely nuclear areas[31] and CIN score (CS) values[32]. To better characterize CIN, we have now combined these complementary, quantitative approaches and applied them in the assessment of CIN from various EOC samples representing various disease states collected over time. Briefly, changes in nuclear areas typically correlate with large-scale alterations in DNA content (*i.e.* ploidy), while a CS is a metric devised to describe gains and losses of three specific chromosomes within a sample that can be associated with both small- and large-scale gains. CS values are determined using fluorescence *in situ* hybridization (FISH) and chromosome enumeration probes (CEPs) for specific centromeres (*e.g.* chromosomes 8, 11 and 17), to assess their presence within samples. Because centromeres are essential chromosome elements, the number of FISH signals (foci) present within a nucleus is indicative of chromosome copy numbers. Accordingly, deviations from two FISH signals/chromosome/cell identify aneuploid cells, or those exhibiting CIN[32]. Thus, unlike the traditional approaches, this novel single cell approach is uniquely capable of quantifying CIN in hundreds of cells both within and between samples over time.

In this study, we employed quantitative imaging microscopy to evaluate CIN (i.e. nuclear areas and CS values) within serial samples isolated from the ascites of EOC patients and within two established EOC cell line models of platinum resistance (PEO1 and PEO4; A2780s and A2780cp). Here we show the patient samples generally harbor increased levels of CIN as reflected by large changes in nuclear areas and CS values. Interestingly, these levels can vary significantly between serial samples indicating aneuploidy and CIN are dynamic in EOC patients and appear to reflect changes in the underlying biology associated with disease status, including responsive, resistant and recurrent disease. By contrast, we show the platinum resistant cell lines exhibit similar levels of CIN, as demonstrated by similar nuclear areas and CS values, suggesting they harbor similar levels of CIN. Collectively, these data suggest that nuclear area and CS values may be useful biomarkers capable of tracking and monitoring disease response and resistance.

Results

CIN is associated with EOC patients samples

To determine whether CIN was associated with EOC, we employed our recently established approaches[31, 32] and assessed CIN using primary cancer cell samples isolated from patient

ascites ([S1 Table](#)). Production of ascites is dependent on the individual patient, and its production often changes throughout the course of the disease and with treatment response[33, 34]. Primary cell samples were labeled with CEPs 8, 11 and 17, counterstained with DAPI and subjected to quantitative imaging microscopy, where both nuclear areas (DAPI) and CS values were determined for hundreds of cells per sample (see [Materials & Methods](#)) ([Fig 1](#)). Six serial samples were isolated and analyzed from EOC18, who was diagnosed with ovarian adenocarcinoma and refused chemotherapy ([Fig 2A](#)). In general, there was a striking degree of heterogeneity observed for nuclear areas within each of the samples ([Fig 2B](#)). The minimum total range observed was 726μm^2 (sample D), while the maximum range was 2794μm^2 (sample H). In addition, the mean nuclear areas were similar within the first five samples (B, 640μm^2; C, 615μm^2; D, 584μm^2; E, 663μm^2; H, 676μm^2), but increased 1.35-fold within the final sample (I, 866μm^2) ([S2 Table](#)). Similarly, the interquartile ranges ([Fig 2B](#), left), which reflect the heterogeneity within a population were also largely overlapping within the first five samples, and increased within the sixth ([S2 Table](#)). [Fig 2B](#) (right) shows that the distribution of sample I was both visually and statistically ([S3 Table](#)) distinct from all other samples. Thus, these data show there is considerable nuclear area heterogeneity within EOC18 that increases with time and disease progression.

Next, CS values were compared between samples from EOC18 (see [Materials & Methods](#)). Briefly, a CS describes both the gains and losses of fluorescent CEP foci within diploid nuclei from a given sample. Under normal conditions, a diploid nucleus harbors two foci per CEP ([Fig 1A](#)), while aneuploid cells will deviate ([Fig 1B](#); [S1 Fig](#)). By definition, CS values reveal deviations from the diploid state (operationally set to 0) as diploid cells have CS values = 0, whereas aneuploid cells have CS values that deviate from 0 ([Fig 1](#); [S1 Fig](#)). FISH was performed, and in agreement with the nuclear areas detailed above, the overall CS_C distribution ranges ([Fig 2C](#), left) were largely overlapping within the first five samples (B to H) (CS_C values typically ≤ 8) and were largest within the final sample (maximum CS_C value = 24). Two sample Kolmogorov-Smirnov (KS) tests comparing the CS_C distributions revealed that all pairwise combinations involving sample I were statistically different (p-value <0.05), while all other pairs were not significant ([S4 Table](#)). Similar trends were also observed for the individual CS values ([Fig 2D and 2E](#)), as KS-tests revealed that all but one of the CS_8, CS_{11} or CS_{17} pairwise combinations involving sample I were significant ([S4 Table](#)). Collectively, these data show that CIN (as measured by nuclear areas and CS values) is present in all EOC18 samples, and further show that CIN remains relatively stable within the first five samples (B to H; ~2 months), but begins to increase within the final sample (I).

CIN is dynamic following carboplatin and paclitaxel treatments

The above observations suggest changes in CIN may reflect alterations in the underlying biology associated with disease progression. To assess whether CIN exhibits distinct temporal dynamics after the patient has received chemotherapy, CIN was evaluated in EOC73, a patient with an ovarian carcinosarcoma whose samples were collected post-carboplatin/paclitaxel treatment ([Fig 3A](#)). As predicted, nuclear area analyses revealed large and dynamic total distribution ranges and mean nuclear areas within each sample ([Fig 3B](#); [S2 Table](#)). This is further illustrated in [S2A Fig](#), which shows largely non-overlapping and statistically distinct cumulative nuclear area distribution frequencies for each sample ([S5 Table](#)). CS_C values were also evaluated and generally show distinct distribution profiles within each sample ([Fig 3C](#)). Large overall ranges were observed in each sample (CS_C values typically ≤ 8) indicating a high prevalence of aberrant numbers of chromosomes 8, 11 and 17. The cumulative CS_C distribution frequencies ([S2B Fig](#)) mirror the nuclear area data, and with the exception of samples C and H,
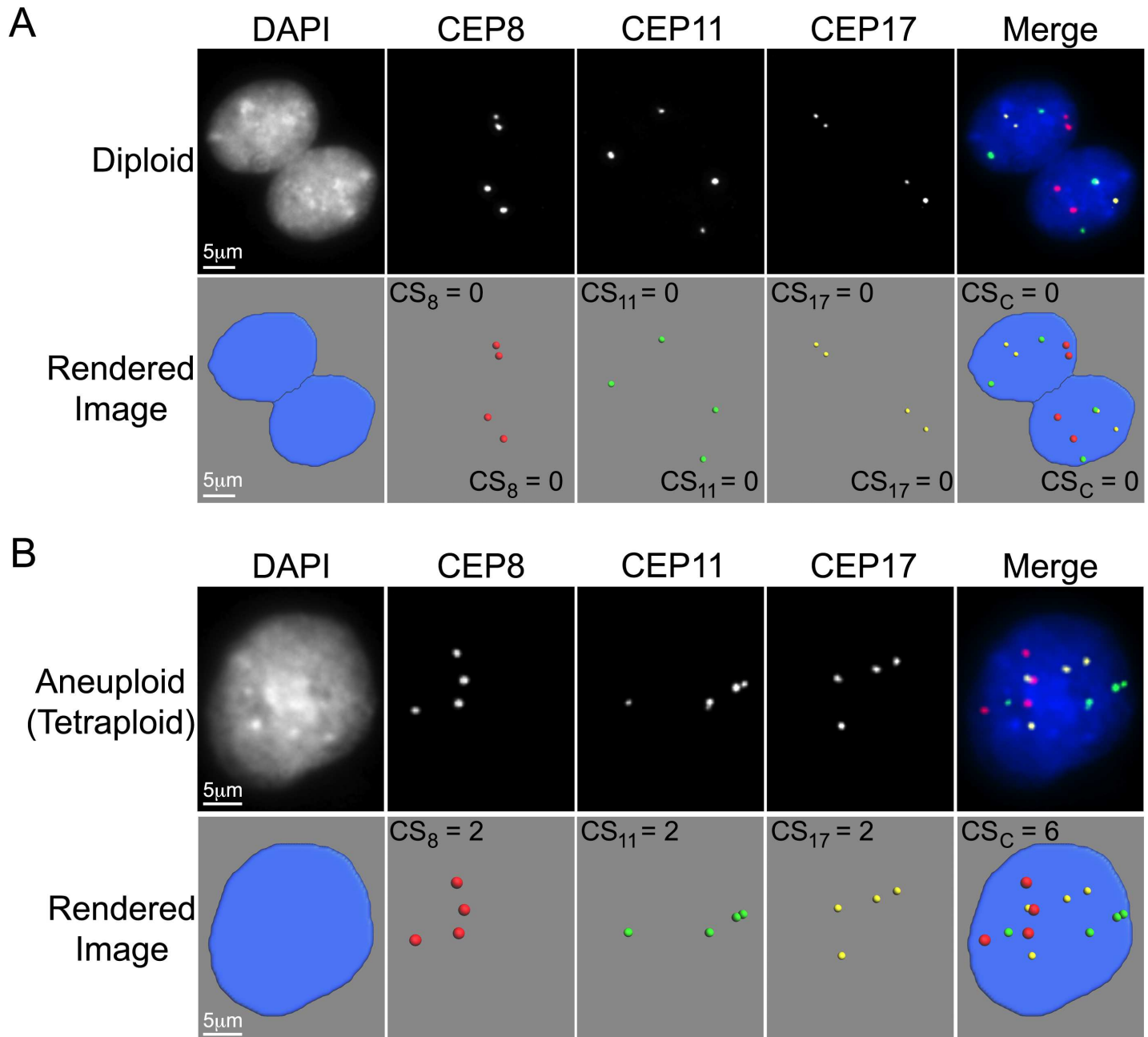
Fig 1. Images Depicting Diploid and Aneuploid States within Primary EOC Cells. (A) Representative high resolution images presenting two diploid EOC nuclei counterstained with DAPI (blue) and labeled with CEPs 8 (red), 11 (green) and 17 (yellow). Presented are the widefield fluorescence images (top) and the corresponding rendered images (bottom) generated and employed to assess both nuclear areas and CS values. Note that within each nucleus, two foci per chromosome evaluated are present indicating the cells are diploid for chromosomes 8, 11 and 17. For illustrative purposes, the individual (CS_8, CS_{11} and CS_{17}) and combined CS (CS_C) values have been included within each rendered image. **(B)** Representative high resolution, widefield fluorescence images (top) and the corresponding rendered images (bottom) of an aneuploid nucleus. Note that four foci are present for each CEP evaluated indicating the cell is tetraploid for chromosomes 8, 11 and 17. For illustrative purposes, the CS values have been included within each rendered image.

all remaining pairwise comparisons are statistically distinct (S6 Table). As expected, similar, albeit less distinct trends were also observed for the individual CS values (Fig 3D; S2C Fig). KS-tests reveal that CS_8 values were the most different between samples, while CS_{11} and CS_{17}
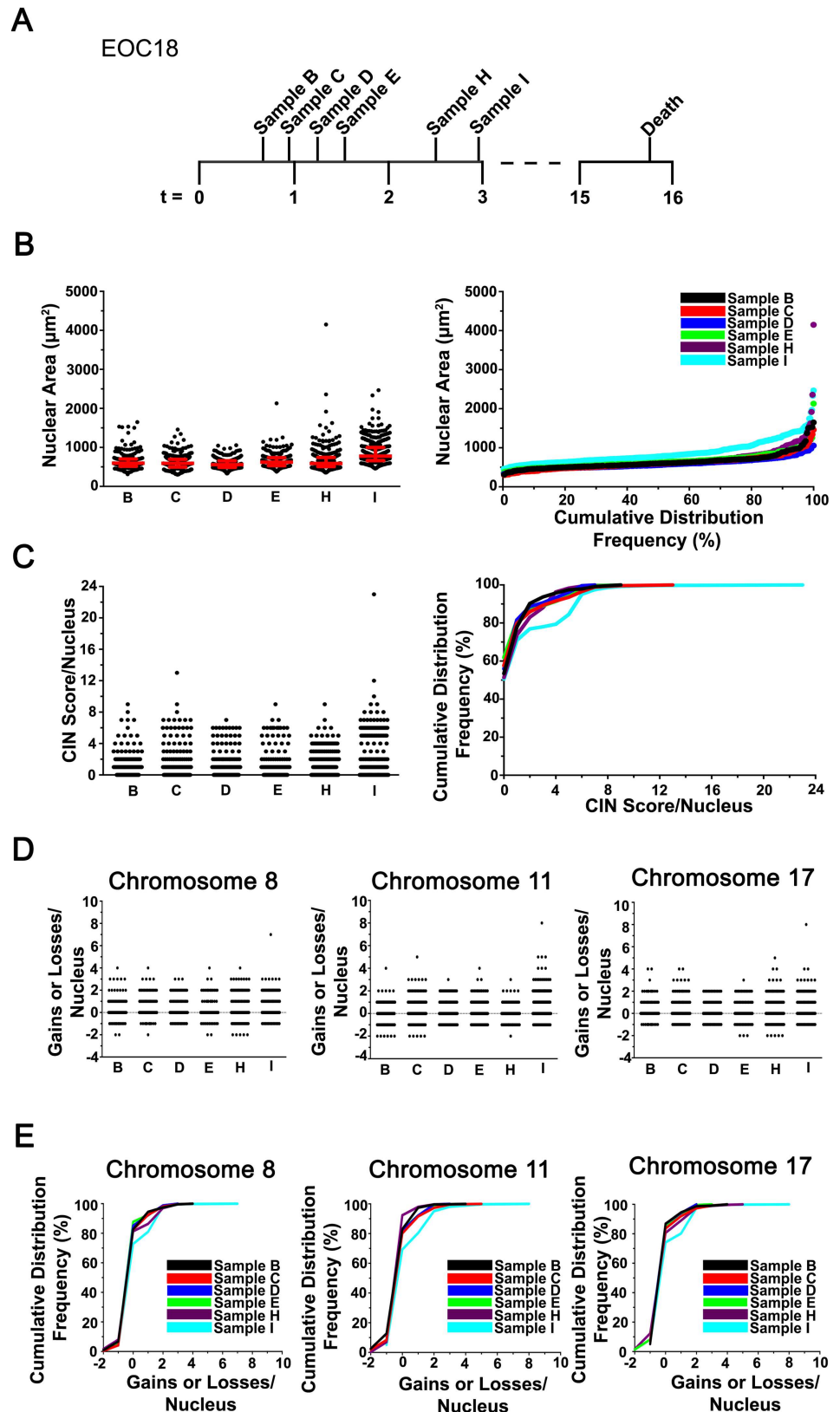
Fig 2. CIN is Associated with Primary EOC. (A) Timeline (months) presenting the six collection times (samples B, C, D, E, H and I) from patient EOC18 (who declined treatment options) prior to death. **(B)** Scatter

plot (left) presenting the nuclear area distributions (black circles) and the associated interquartile ranges (25th, 50th and 75th percentiles; red horizontal lines). Cumulative distribution frequency graph (right) depicting nuclear areas arranged from smallest to largest. **(C)** A scatter plot (left) presenting the CS_C distributions of samples B to I, and the corresponding cumulative CS_C distribution frequencies (right). Note that the absolute values of gains and losses are presented for the combined CS values (CS_C; CEPs 8, 11 and 17), and that a CS_C value of 0 identifies a diploid nucleus for each chromosome evaluated (*i.e.* 2 copies of CEPs 8, 11 and 17). **(D)** Scatter plots presenting the gains and losses in CS_8 (left), CS_{11} (middle), and CS_{17} (right) for each nucleus analyzed within each sample. Note that both gains (positive values) and losses (negative values) are shown for each individual CEP evaluated. **(E)** Cumulative distribution frequency graphs for CS_8 (left), CS_{11} (middle) and CS_{17} (right).

values were most similar (S6 Table). Collectively, the above data show CIN is dynamic following carboplatin/paclitaxel treatments and initially decreases (sample B to G) before increasing (sample H), implying changes in CIN reflect the temporal therapeutic effects and tumor response to chemotherapy.

CIN increases in resistant recurrent disease

The preceding sections suggest CIN may be a novel biomarker that reflects changes associated with disease progression, recurrence, and/or drug treatments. To assess this possibility, CIN was evaluated in samples isolated from EOC13 (Fig 4A) and EOC140 (Fig 5A), patients diagnosed with recurrent, platinum-resistant HGSOC. Nuclear areas were assessed as above (S2 Table), and visually distinct differences in the distribution ranges were apparent for both patients (Figs 4B and 5B). EOC13 exhibited an overall increase in the total distribution range from sample A to D that decreased in sample F. Statistically significant increases in mean nuclear areas were also observed in samples C and D (752μm^2 and 849μm^2, respectively) relative to sample A (520μm^2), that was followed by a statistically significant decrease within sample F (677μm^2). Despite the decrease in mean nuclear area within sample F, the interquartile ranges continued to expand and was largest in sample F (Fig 4B). Finally, KS-tests comparing the cumulative nuclear area distribution frequencies (see S3A Fig) reveal all pairwise combinations were statistically distinct (S7 Table). For EOC140, Fig 5B shows that the overall nuclear areas and interquartile ranges were large, generally distinct between samples, and were typically associated with increases in mean nuclear areas apart from samples B to C and D to E (S2 Table). Further, all pairwise combinations evaluating the cumulative nuclear area distribution frequencies (S4A Fig) were statistically distinct (S8 Table) with the exception of samples D and E.

Next, CS values were evaluated and large CS_C ranges were observed within each EOC13 sample (Fig 4C; CS_C values typically ≤ 8) that subsequent KS-tests revealed were statistically significant (S3 Fig and S9 Table). Similar trends occurred for CS_8, CS_{11}, and CS_{17} (Fig 4D), and KS-tests revealed that most pairwise comparisons were statistically different with the exception of A versus F for both CS_8 and CS_{17}, and D versus F for CS_{17} (S9 Table). Similarly, the CS_C values were also dynamic in EOC140 (Fig 5C), however they were generally larger (typically ≤ 20) with maximal values ranging from 30 and 35 in samples B to G, indicating high levels of aneuploidy and CIN. This trend was also observed for the cumulative distribution frequencies (S4B Fig) and was further highlighted by the significant KS-tests for all pairwise comparisons with the exception of samples C vs. D and D vs. E (S10 Table). In agreement with the CS_C values, CS_8, CS_{11} and CS_{17} values exhibit similar dynamic patterns (Fig 5D) with largely distinct distribution patterns observed between samples (S4C Fig; S10 Table). The apparent difference observed between nuclear areas and CS values for EOC140 may suggest that while many chromosomes are dynamically gained or lost, overall there may be selective pressures that maintain or promote selective gains in chromosomes 8, 11 and 17 (Fig 5D).
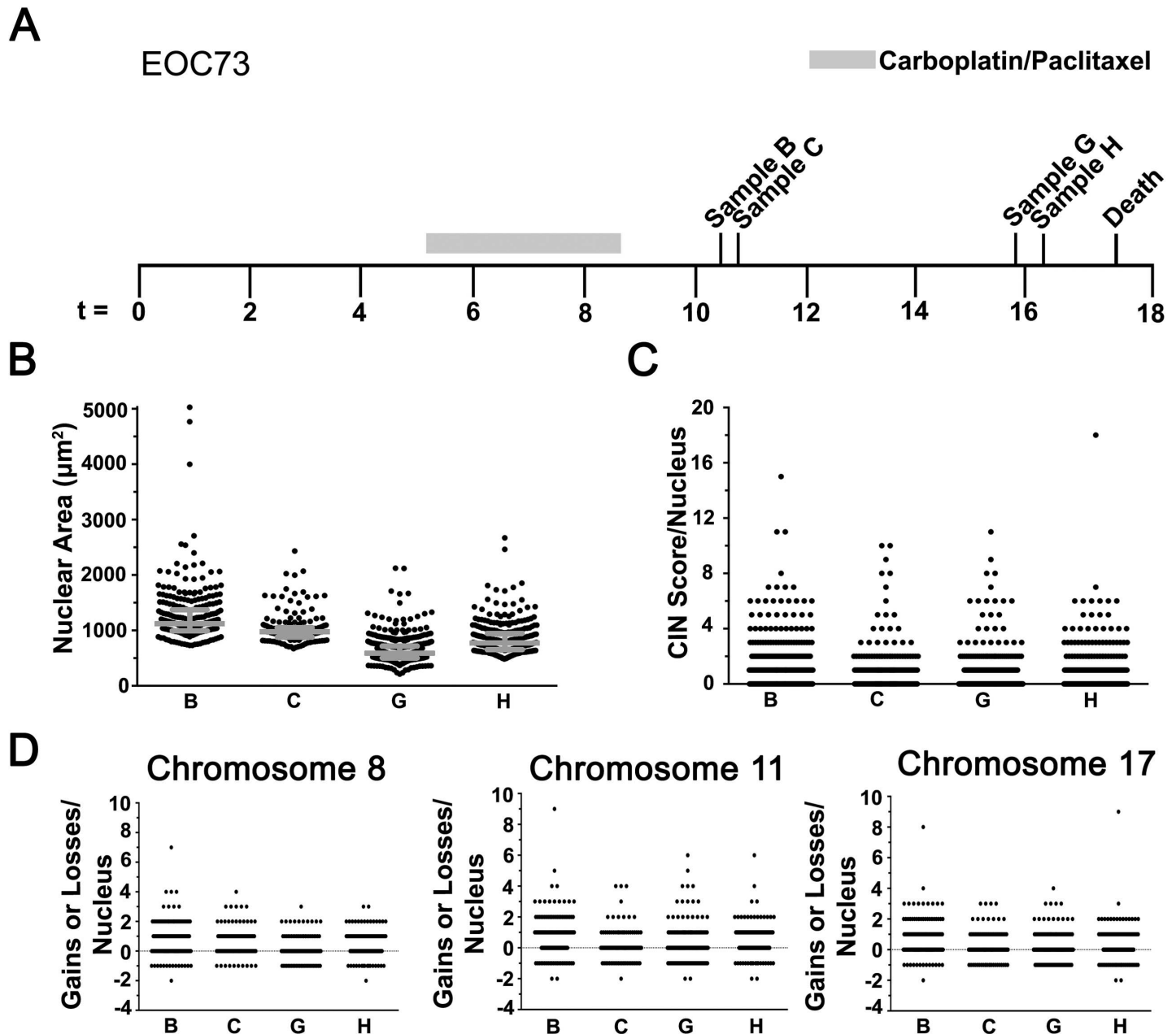
Fig 3. CIN is Dynamic and Changes in Response to Frontline EOC Chemotherapy. (A) A timeline (months) presenting the collection times for samples B, C, G and H from EOC73 relative to Carboplatin/Paclitaxel treatment. **(B)** Scatter plot depicting the nuclear area distribution for each sample with the interquartile ranges indicated in grey. **(C)** Scatter plot depicting the CS_C values for each nucleus evaluated within the indicated samples. **(D)** Scatter plots presenting the gains and losses in CS_8 (left), CS_{11} (middle) and CS_{17} (right) for each nucleus analyzed within sample.

https://doi.org/10.1371/journal.pgen.1006707.g003

Taken together, the above data show that CIN is prevalent and highly dynamic within EOC140. They further show that high levels of aneuploidy and CIN are present within recurrent disease and that further treatments (*i.e.* Caelyx) did not impact the overall size of nuclei nor the CS values within the bulk of the cells evaluated within the samples. These data again show that CIN is dynamically associated with EOC, further supporting its potential utility as putative biomarker.
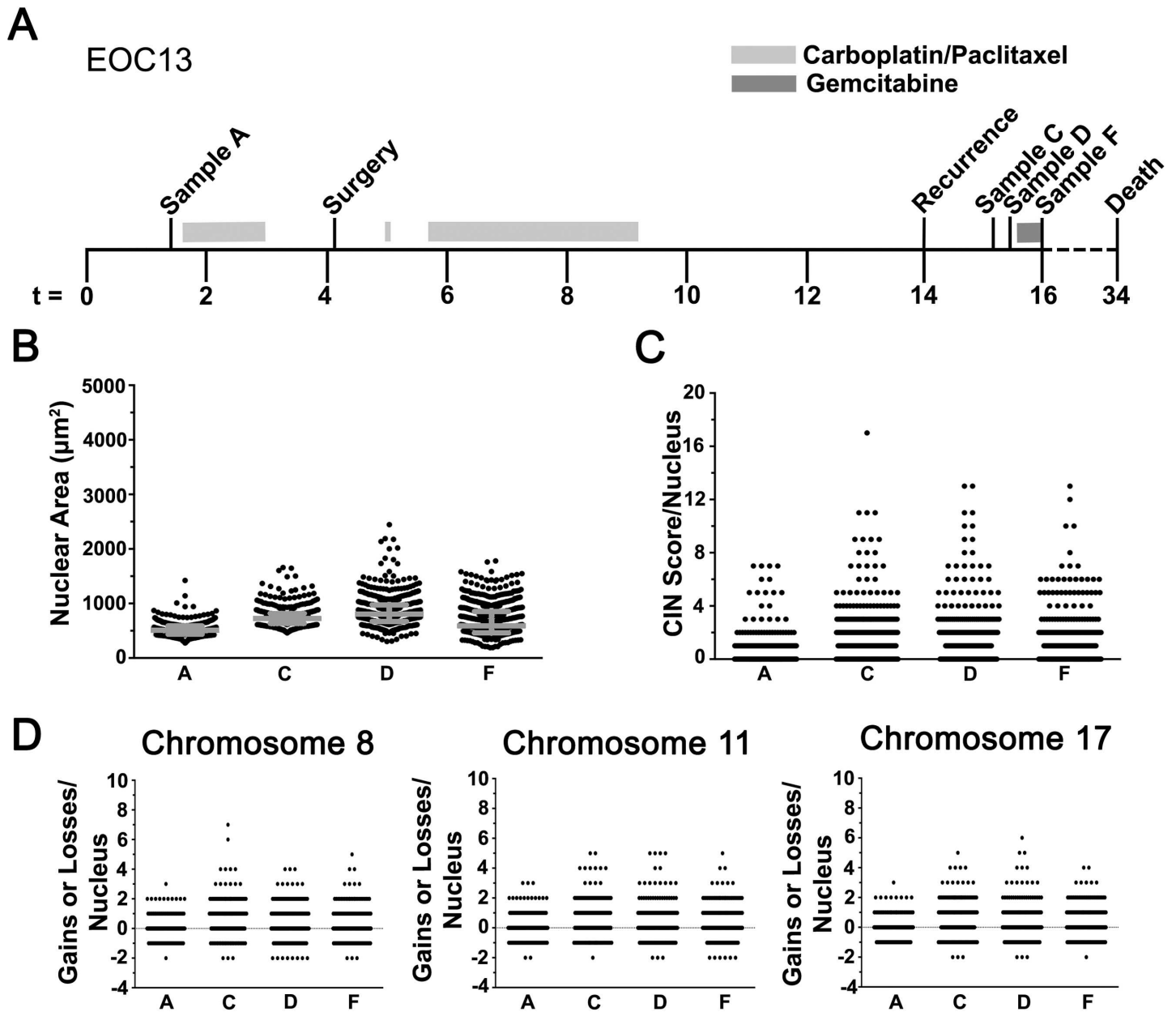
Fig 4. CIN Increases in Recurrent Disease. (A) Timeline (months) indicating the time of collection for samples A, C, D and F from patient EOC13 relative to treatments, surgery and recurrence. **(B)** Scatter plot depicting the nuclear area distributions and interquartile ranges (grey). **(C)** Scatter plot presenting the overall distribution of CS_C values within each sample. **(D)** Scatter plots for each of the individual CS values; CS_8 (left), CS_{11} (middle) and CS_{17} (right).

Increases in CIN are associated with the development of platinum resistant EOC

CIN is associated with the acquisition of multi-drug resistance in numerous cancer types[14–17], but there is a paucity of data regarding its association with platinum resistant EOC. The findings of the preceding section show CIN is dynamic, and predict high levels of CIN will be associated with platinum resistance (*e.g.* EOC140). To explore this possibility, CIN was evaluated in samples from EOC16 (Fig 6A), a patient with platinum resistant disease who was
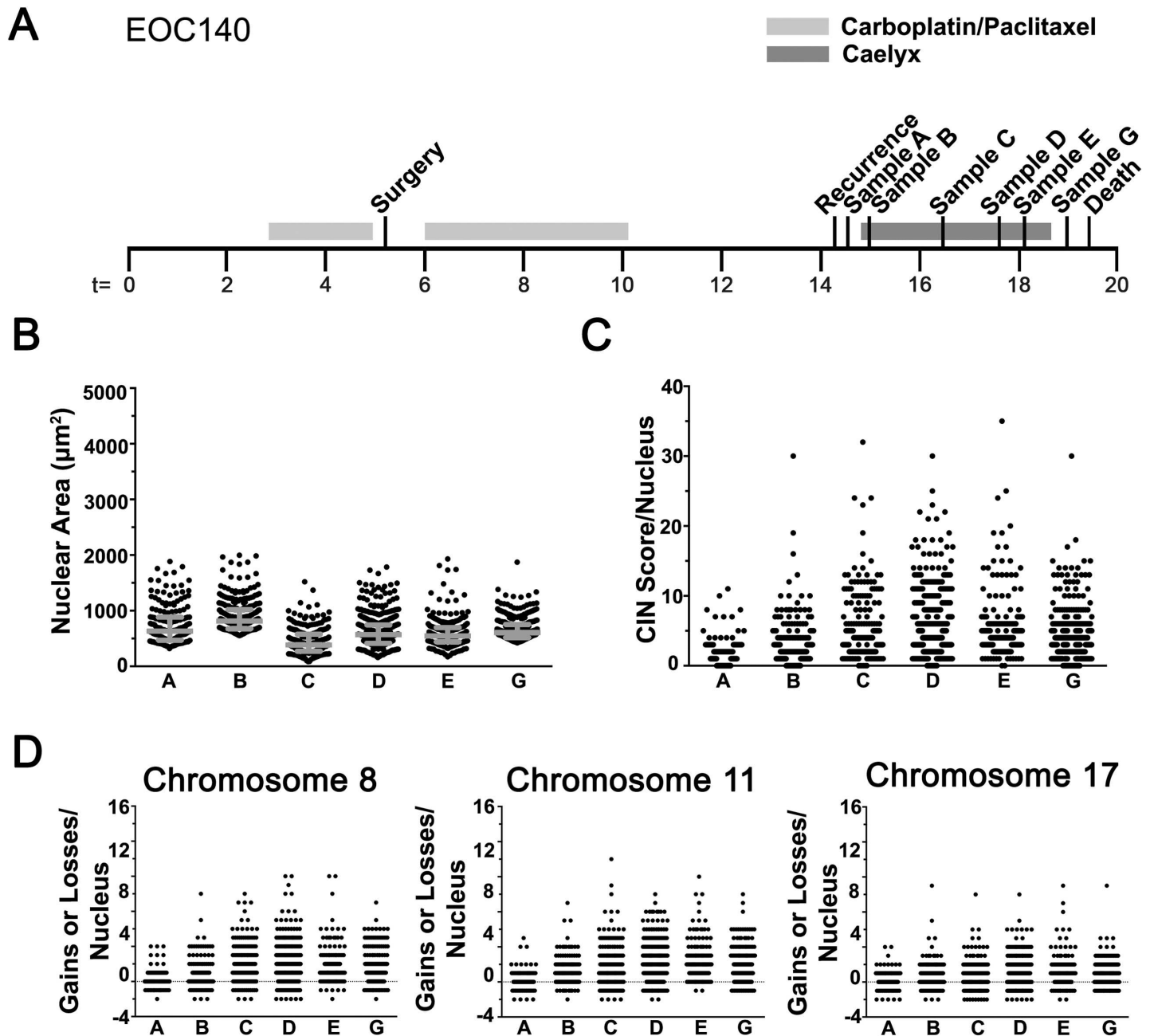
Fig 5. Extensive Levels of CIN are Associated with Recurrent Disease. (A) Timeline (months) presenting the collection times of the six samples collected from patient EOC140 relative to surgery, disease recurrence and death. **(B)** Scatter plot presenting the overall distribution of nuclear areas from each sample with the interquartile range indicated in grey. **(C)** Scatter plot of CS_C values. Note the expanded range for the overall distributions. **(D)** Scatter plots presenting CS_8 (left), CS_{11} (middle) and CS_{17} (right) for each nucleus evaluated.

https://doi.org/10.1371/journal.pgen.1006707.g005

administered Caelyx prior to death. Similar to the platinum resistant samples analyzed above, increases in nuclear area were associated with the acquisition of resistance, or given the rapid progression of the disease, enrichment of platinum resistant cells (Fig 6B). More specifically, increases in the interquartile ranges were observed in samples F and G relative to sample B that were accompanied with significant increases in mean nuclear areas (S2 Table). Surprisingly, sample H (undergoing Caelyx treatment) maintained a large interquartile range despite

showing a significant decrease in mean nuclear area relative to sample G (prior to Caelyx treatment). The cumulative nuclear area distribution frequencies (S5A Fig) of the three post-treatment samples appeared similar and distinct from the pre-treatment sample (B), which KS-tests showed were statistically distinct (S11 Table).

In general, the CS_C values closely parallel those of the nuclear areas (Fig 6C; S5B Fig) as the CS_C values were generally larger (typically ≤ 20) than those of all EOC patient samples evaluated thus far (typically ≤ 8), and were as high as 45 to 93 in samples F, G and H indicating extreme levels of aneuploidy and CIN (S1 Fig). Similarly, the individual CS values exhibited dynamic patterns over time (Fig 6D) as the CS_8, CS_{11} and CS_{17} values increased from sample B to G and decreased marginally within sample H. Further, CS_8, CS_{11} and CS_{17} values were maximal in sample G and decreased within sample H, but still exhibited the greatest levels of aneuploidy as indicated by the right-shifted cumulative distribution curve (S5C Fig). Subsequent KS-tests revealed all pairwise combinations were statistically distinct with the exception of sample F versus G for both CS_8 and CS_{17} (S12 Table). Collectively, these data confirm CIN is both prevalent and dynamic in HGSOC, and further show high levels of CIN are associated with platinum resistance and that Caelyx treatments do not appear to significantly impact nuclear size nor CS values in EOC16.

Cellular models of drug resistance in EOC exhibit similar levels of CIN

We next sought to determine whether CIN was also associated and dynamic in two paired EOC models of drug resistance, PEO1/PEO4 and A2780s/A2780cp. PEO1 (sensitive) and PEO4 (resistant) cells were isolated and derived from a single EOC patient with HGSOC pre- and post-platinum resistance[35], while A2780cp (resistant) cells were derived through dose escalation in the cisplatin sensitive parental line (A2780s) isolated from a patient with ovarian clear cell carcinoma[36]. Nuclear areas were quantified as above and in stark contrast to the patient samples, PEO1/PEO4 cells exhibited relatively small overall distribution and interquartile ranges (Fig 7A; S13 Table). In fact, there was a small ~1.3-fold decrease in mean nuclear area within PEO4 cells ($391\mu m^2$) compared to PEO1 ($510\mu m^2$) along with a significant decrease in the cumulative distribution frequency (KS-test; p-value < 0.0001) (S6A Fig). Similarly, the overall and interquartile ranges were small within A2780s and A2780cp cells (S7A Fig; S13 Table), however there was a modest, albeit statistically significant, increase in cumulative nuclear area distribution frequency (KS-test; p-value $= 0.001$) within A2780s relative to A2780cp (S7A Fig). Next, CS_C values were calculated and revealed small overall distribution ranges that were typically ≤ 4 (Fig 7B; S7B Fig). In addition, the cumulative distribution frequencies were largely superimposable and not statistically distinct for either PEO1/PEO4 (p-value < 0.88) or A2780s/A2780cp (p-value $= 0.10$). Similarly, the CS_8, CS_{11} and CS_{17} distribution ranges were also largely overlapping (Fig 7C; S7C Fig) as were the cumulative distribution frequencies (S6C Fig; S7D Fig). Collectively, these data show that the paired cell line models exhibit small, yet similar nuclear area distributions and CS values, indicating that the sensitive and resistant cell lines exhibit similar levels of CIN.

Mean CS values are dynamic and high within aggressive disease

To compare CIN between EOC patient samples and the paired drug resistant lines, mean CS (mCS) values were calculated[32]. For reference purposes, a mCS = 0 is indicative of a diploid population, whereas a mCS value >0 identifies an aneuploid population. As shown in Fig 8, the mCS values calculated for each of the initial EOC patient samples was <2, and ranged from 0.499 (EOC13) to 1.675 (EOC73). Interestingly, the mCS value remained relatively static in subsequent samples evaluated from EOC13, EOC16, and EOC140, while those in EOC73
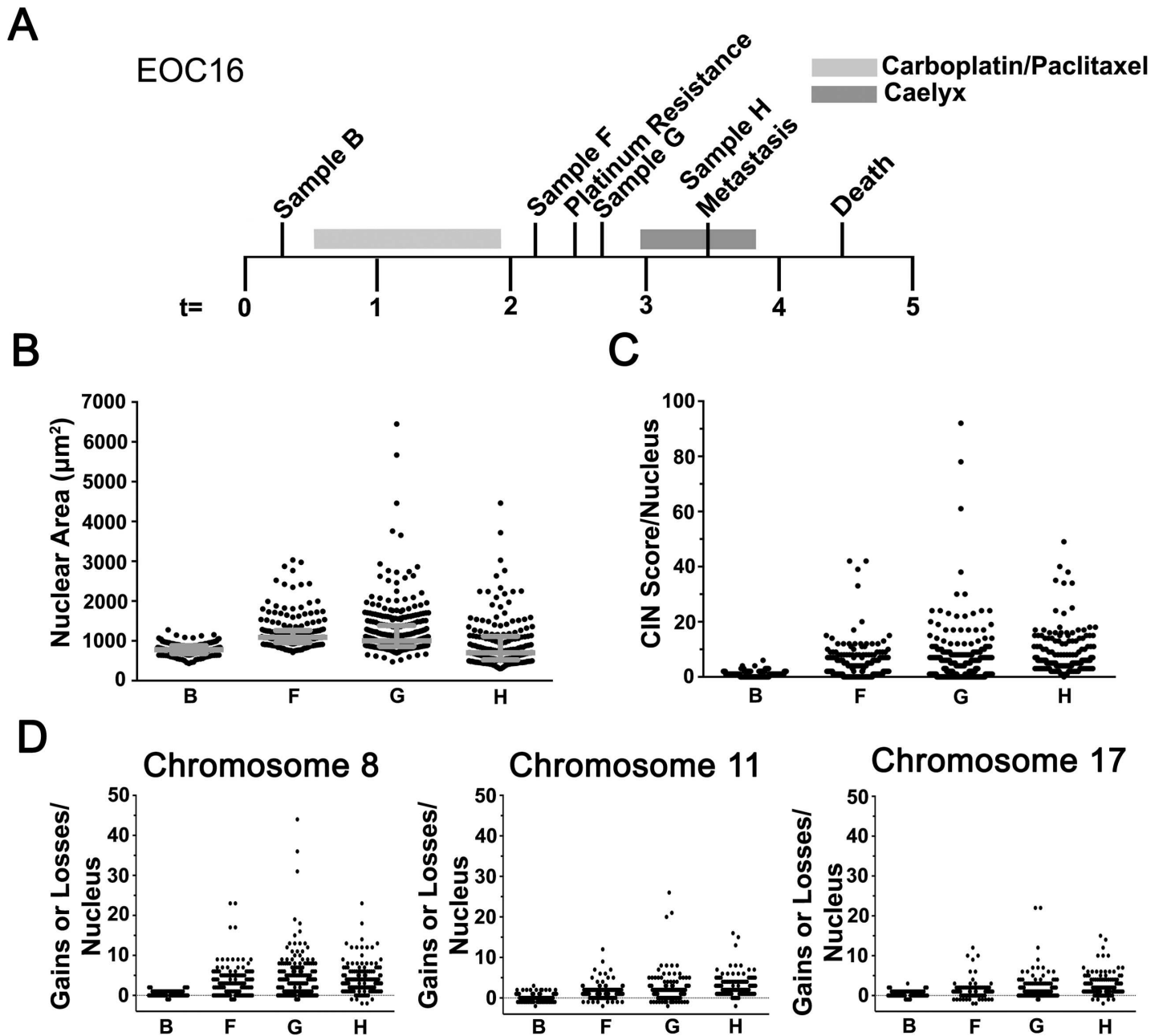
Fig 6. The Levels of CIN Increase in Aggressive and Platinum Resistant Disease. (A) Timeline (months) indicating the collection times for samples B, F, G and H from patient EOC16 relative to treatments, platinum resistance, metastasis and death. **(B)** Scatter plot for nuclear areas from the indicated samples (interquartile ranges indicated in grey). **(C)** Scatter plot for the CS_C values. **(D)** Scatter plots presenting the overall distribution of CS_8 (left), CS_{11} (middle) and CS_{17} (right) from each nucleus evaluated within the indicated samples.

https://doi.org/10.1371/journal.pgen.1006707.g006

and EOC18 were dynamic. More specifically, the mCS value from EOC18 (refused treatment) were stable for the first four samples before increasing within the final two samples (1.1 and 1.7). Conversely, the mCS values of EOC16 and EOC140 increased dramatically in the second and third samples, respectively, and remained high (mCS >4) in all subsequent samples. The above data predict the drug resistant cell lines, PEO4 and A2780cp will have elevated mCS values relative to the paired sensitive lines. Interestingly, although the sensitive lines have mCS
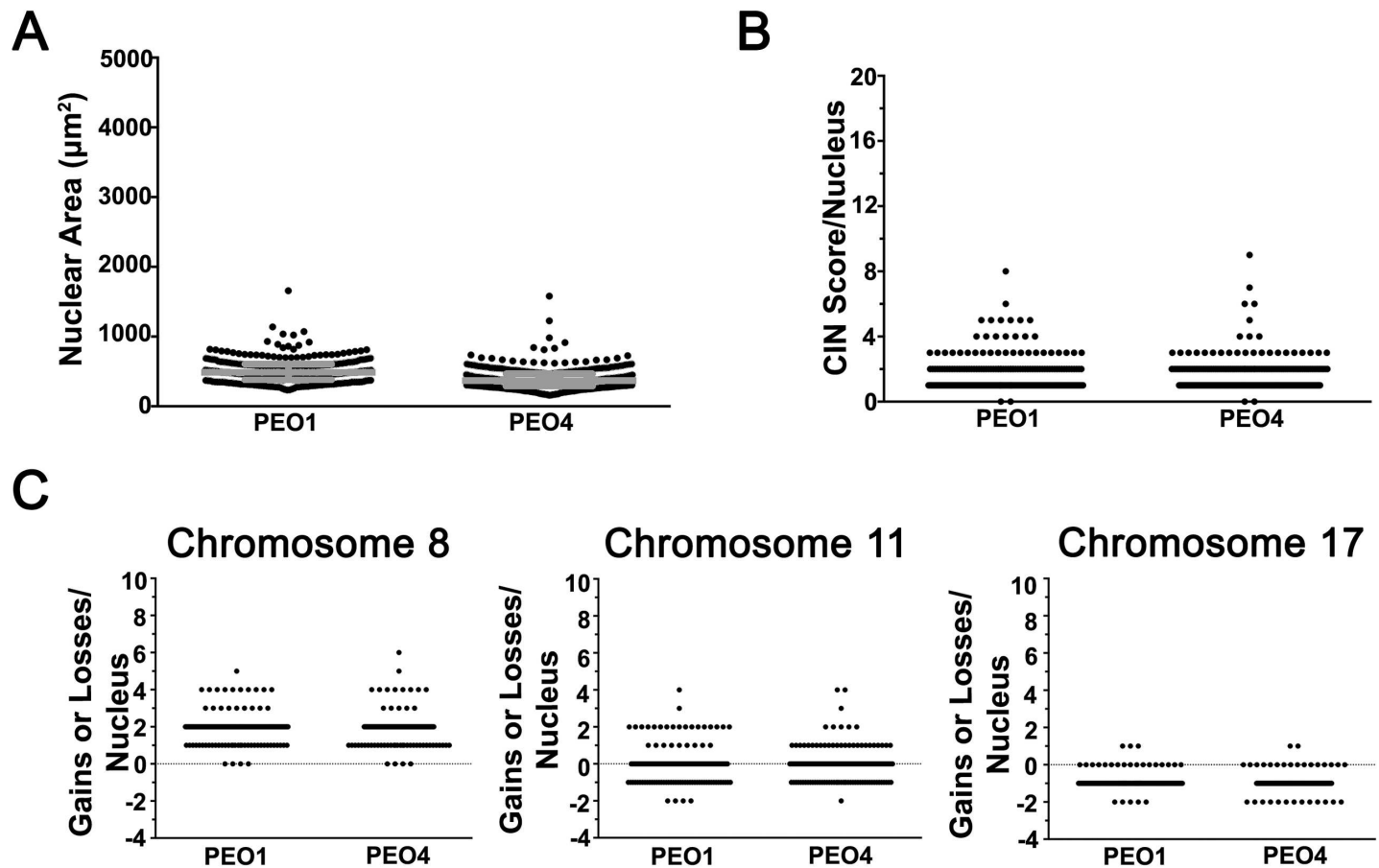
Fig 7. PEO1 and PEO4 Cells Harbor Similar Levels of CIN. (A) Scatter plot depicting the nuclear area distribution for PEO1 (sensitive) and PEO4 (resistant) cells with the interquartile ranges (25th, 50th and 75th percentiles) identified in grey. **(B)** Scatter plot depicting the CS_C distribution for nuclei in PEO1 and PEO4 cells. **(C)** Scatter plots presenting the gains and losses of CEP 8 (CS_8; left), 11 (CS_{11}; middle) and 17 (CS_{17}; right) for each nucleus analyzed in PEO1 and PEO4.

https://doi.org/10.1371/journal.pgen.1006707.g007

values (PEO1 = 1.547; A2780s = 0.538) that are comparable to those of the initial EOC patient samples, the mCS values are lower in the corresponding drug resistant lines (PEO4 = 1.426; A2780cp = 0.316). Overall, the above results show that mCS values remain relatively low (mCS <2) in stable and responsive disease, but increase dramatically within resistant or aggressive disease suggesting mCS values are a novel candidate biomarker capable of monitoring disease progression and response.

Discussion

To glean unprecedented insight into the prevalence and dynamics of CIN in EOC patient samples and two ovarian cancer cell models of drug resistance, we combined our recently developed analyses[31, 32] and assessed two surrogate markers of CIN. Using quantitative, single cell imaging approaches we show CIN, as characterized by changes in nuclear areas and CS values, is associated with all EOC samples, and further show it is dynamic and increases in resistant, recurrent disease. A constraint of the current study is that it is drawn from small patient cohorts, which limits the power of the study to draw firm conclusions about the temporal dynamics of CIN until additional samples can be acquired and analyzed. Nevertheless, the results of the current study suggest that alterations in CIN may reflect the underlying genetic
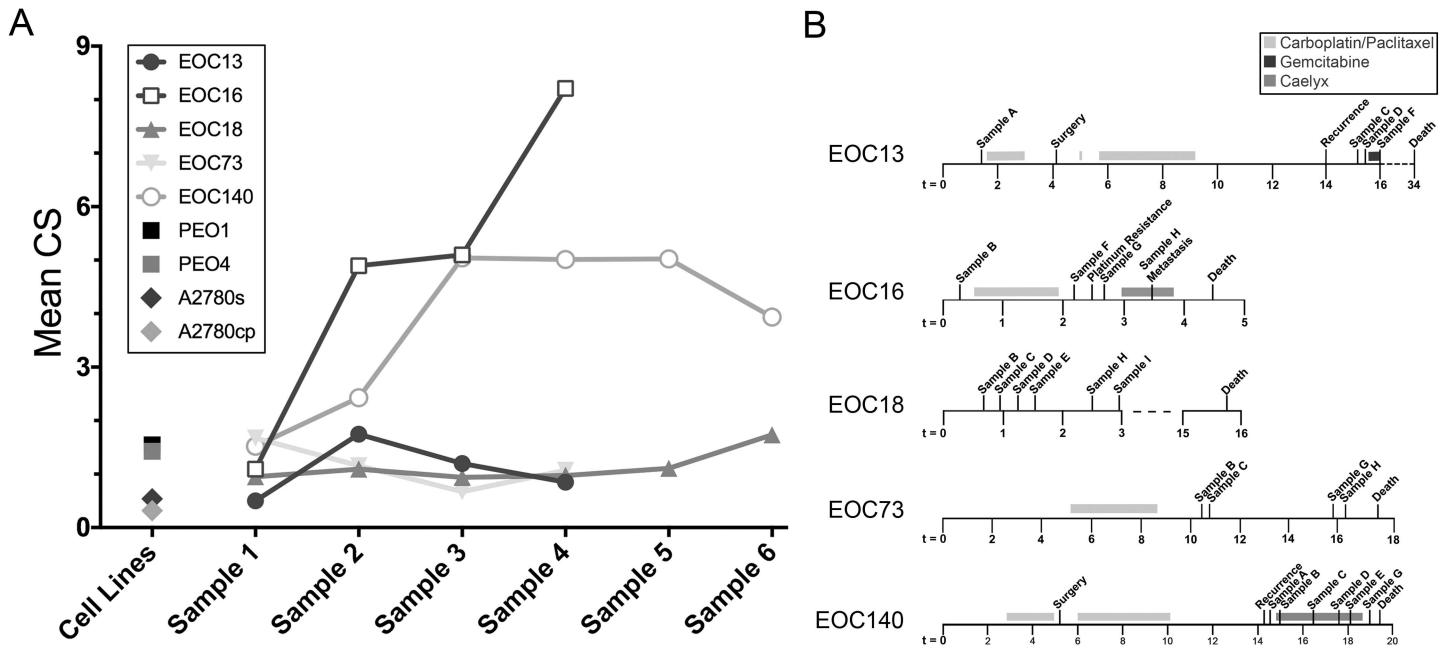
Fig 8. Mean CS Values in Primary EOC Patient Samples and Cell Line Models. (A) Graph presenting the mCS values calculated for each patient and sample isolated from each patient, and those of the paired EOC cell line models (PEO1/PEO4 and A2780s/A2780cp). Note that the mCS value in each of the initial patient samples is <2 and remains low in all subsequent samples with the exception of EOC16 and EOC140, which exhibit striking increases in mCS values prior to succumbing to the disease. Also, note that the carboplatin resistant cell lines (PEO4 and A2780cp) both exhibit small decreases in mCS values relative to their sensitive counterparts. **(B)** Timelines presenting the sample collection times for each EOC patient presented in **(A)** relative to disease progression and treatment(s).

changes driving disease progression and drug response. For example, significant differences in mean nuclear areas and CS values occurred in serial samples collected from EOC patients, particularly those undergoing chemotherapy. Results from EOC73 (Fig 3) demonstrate CIN decreases following the initial carboplatin/paclitaxel treatments before increasing within the final sample. Similarly, CIN increases prior to, and immediately following, platinum resistance in EOC16 (Fig 6), but decreases slightly following Caelyx treatments. These data reveal a potential association between platinum resistance and increases in CIN (*i.e.* increased heterogeneity). In support of this possibility, CIN remains relatively stable in EOC18 (Fig 2), an individual who refused all treatments. In fact, nuclear areas and CS values remained relatively constant within the first five samples, but increased within the final sample as the disease progressed. Collectively, these observations raise the question of whether changes in CIN reflect the pathologic changes driving disease progression, or those induced by drug treatments.

In agreement with these findings, both cellular models of drug resistance exhibit CIN; however, both models show remarkable similarity between the paired sensitive (PEO1 and A2780s) and resistant lines (PEO4 and A2780cp). Despite PEO4 being isolated 10 months after relapse and being platinum resistant[37], we did not observe elevated levels of CIN (*e.g.* nuclear areas and CS values) relative to PEO1. In fact, our data show that PEO1 and PEO4 are similar with respect to nuclear areas and CS values (Fig 7). Although our approach is incapable of detecting segmental aneuploidy (*i.e.* gains or losses in portions of chromosomes), our data indicate that chromosomes 8 and 17 are preferentially gained and lost in PEO1 and PEO4, respectively (Fig 7C). Thus, our data show that although PEO1 and PEO4 share many features of CIN, the PEO4 cells typically exhibit less heterogeneity in nuclear areas and CS values. As with the PEO1/4 cells, the A2780s/cp cells also exhibited similar levels of CIN as demonstrated

by largely superimposable cumulative nuclear area distribution frequencies (S7 Fig). Accordingly, unlike the increases in CIN observed within the drug resistant EOC samples (*e.g.* EOC13, EOC16 and EOC140), CIN does not increase within the drug resistant cell lines. Thus, our study challenges the suitability of the PEO1/4 and A2780s/cp cell models to accurately reflect the aberrant biology observed in the EOC patient samples, specifically with respect to CIN and drug resistance. While surprising, the markedly similar levels of CIN may simply reflect the artificial selection pressures employed to derive and maintain the cell lines, including 2D growth on plastic and extensive culturing. Consequently, the results of this study caution the use and interpretation of results relating drug resistance and CIN derived from the PEO1/PEO4 and A2780s/A2780cp models, and support the use of primary cultures or the development of more representative cellular models[38].

While many studies have shown genome instability is a common feature of EOC[20–29], none have adequately characterized CIN within patient samples or cell lines, particularly in samples collected over time. Typical studies employ karyotypic analyses, CGH, SNP analysis, and next generation sequencing to identify numerous gene copy number variations, losses of heterozygosity, and/or structural rearrangements[20–29, 39–48]. Although these studies have provided fundamental insight into EOC, they are limited in scope as they only use endpoint analyses (*i.e.* a single timepoint), and are heavily influenced by population averaging. In fact, these studies typically only ascribe a single consensus karyotype/genotype, and do not describe the extensive heterogeneity that occurs. To assuage these limitations, we recently developed and validated two quantitative, single cell imaging approaches[31, 32] capable of characterizing the heterogeneous nature of CIN within populations, which we combined for the first time in the current study. Thus, this study is the first to employ quantitative, single cell analyses to characterize CIN and evaluate its temporal dynamics in serial EOC samples. Having observed CIN is dynamic and associated with EOC, we propose CIN is a novel candidate biomarker that may be useful for monitoring disease progression and treatment response. As such, it is tempting to speculate that changes in CIN may help identify and/or distinguish those individuals with responsive or resistant disease, which could conceivably impact clinical management. However, before CIN is established as a novel biomarker in EOC, or any other cancer type, more extensive studies incorporating additional samples are required.

Data gleaned from our study show that CIN is dynamic and increases with drug resistant and recurrent EOCs. These findings are in agreement with a large number of studies in a variety of cancer types that show CIN is associated with the acquisition of drug resistance[16, 18, 35, 49]. Paradoxically, there is a body of evidence that suggests increases in genome instability may also be associated with improved biological fitness and survival outcome[20, 50, 51]. Importantly however, the increases in genome instability often described within these studies does not necessarily specifically relate to CIN, and many researchers frequently use these terms interchangeably despite very different classical definitions. Indeed, CIN is only one of several mechanisms proposed to impact genome stability, which may also include defects in the DNA repair response, microsatellite instability and CpG island methylator phenotype. Further, many of the studies relating CIN to survival outcome typically employ next generation sequencing, SNP analyses or CGH to characterize changes in the abundance of gene copy numbers, SNPs or chromosomal segments as proxies for CIN, but do not actually assess chromosome numbers, particularly at the single cell level. Accordingly, these studies are likely identifying the most frequently occurring driver and passenger alterations that do not necessarily involve whole chromosomes or large parts thereof (*i.e.* CIN). While these studies have provided useful insights related to various types of genome instability, they are incapable of characterizing the cell-to-cell heterogeneity in chromosome numbers that is expected to occur in CIN+ (*e.g.* CIN containing) tumors. For example, these studies typically employ combined

DNA extracted from large cellular populations (*e.g.* 10^3 to 10^6 cells) and are inherently incapable of detecting or characterizing subtle differences in chromosome numbers predicted to occur in a heterogeneous population of CIN+ tumor cells. Finally, and perhaps most importantly, none of the previous studies have specifically evaluated the temporal kinetics of CIN within a given EOC patient over time or in response to drug treatments, disease recurrence and resistant disease. Thus, the approach employed in the current study provides several novel and key advancements over more traditional approaches.

In general, there is good concordance between the nuclear areas and CS values calculated for each of the EOC patients and the paired cell line models. However, there are instances where the two metrics appear to differ (see EOC140; Fig 5). Although uncommon, this can be expected and likely reflects the inherent differences in the sensitivity of each approach, and is precisely why these approaches have been combined. For example, significant changes in nuclear areas are most likely to reflect large scale changes in DNA content (*i.e.* tetraploidy), rather than small scale changes associated with the gain or loss of small subsets of chromosomes (*i.e.* 1 or 2 chromosomes). Conceivably, these large scale changes could be envisioned to occur as a result of chromosome segregation defects that may occur following mitotic checkpoint escape, and result in the formation of a tetraploid nucleus. On the other hand, significant differences in CS values are expected to reflect both small and large scale changes in chromosome numbers, provided those changes involve at least one of the three chromosomes evaluated (8, 11, or 17). However, the CS approach is incapable of discerning subtle differences occurring between a tetraploid cell (i.e. 4 copies of all chromosomes; 92 chromosomes) versus an aneuploid cell (52 chromosomes) harboring 4 copies each of chromosomes 8, 11 and 17. Accordingly, the concordance/discordance observed in nuclear areas and CS values for any given sample may simply reflect an underlying difference in the mechanism(s) giving rise to the CIN phenotype. It is for these reasons we believe the concurrent assessment of both nuclear areas and CS values is critical to assemble a more comprehensive assessment of CIN and its dynamics within EOC patient samples.

Finally, although the current approach monitors CIN in EOC cells isolated from ascites, only ~30% of women with EOC produce ascites. To enhance the utility of this approach, we propose it could be modified and applied to assess CIN in both solid and liquid tumour biopsies. In support of this possibility, we previously developed the CS approach and applied it in mini-tissue array comprised of 141 colorectal cancer samples[32]. Thus, we propose the current approach, with slight modifications, could be applied to evaluate CIN in EOC tissues and circulating tumour cells isolated from peripheral blood. As such, nuclear areas and CS values (i.e. CIN analyses) would have broad implications for EOC and virtually any cancer where biopsy or circulating tumour cells are available. However, the general applicability and utility of this approach in monitoring and predicting disease outcome is premature and requires subsequent studies involving appropriate sample sources (*e.g.* ascites, biopsy or circulating tumour cells).

Materials and methods

Cell culture

Institutional approval for research with human materials was received prior to the initiation of these studies (University of Manitoba Research Ethics Board, #HS19422), and samples were used after receiving informed written consent. Serial ascites obtained by paracentesis from patients with adenocarcinoma was used as a source of primary human EOC cells, and grown as previously described[52]. While numerous primary EOC samples were obtained from patients via paracentesis, some cell samples may not have grown adequately to conduct

experiments. All experiments with primary EOC cells were performed between passages 1 and 3. To determine tumor cell purity within the patient samples, quantitative imaging microscopy was performed using a PAX8 antibody (Abcam; ab189249, 1:200), as all tumor cells will be PAX8+ and all potential contaminating normal mesothelial cells are PAX8-. We confirm that >99% of cells are PAX8+ from each of the EOC samples evaluated (>200 cells/sample). PEO1 and PEO4 are cisplatin sensitive and resistant lines[35], respectively, and were purchased from Sigma-Aldrich. PEO cells were grown in RPMI 1640 supplemented with fetal bovine serum (10%), 2 mM glutamine, and 2 mM sodium pyruvate. The cisplatin sensitive human ovarian carcinoma cell line A2780s, and its cisplatin resistant derivative, A2780cp, were obtained from Dr. B. Tsang (University of Ottawa). Short tandem repeat profiling was employed to authenticate the A2780 cells in June 2016 using the Promega PowerPlex system. All cells, with the exception of the PEO1/4 were cultured in DMEM/F12 (HyClone) supplemented with fetal bovine serum (10%). All cells were maintained at 37˚C, 5% CO_2 and 100% humidity.

FISH

Chromosome enumeration FISH probes (CEPs) specifically recognizing the pericentric regions of chromosomes 8 (CEP8; SpectrumOrange), 11 (CEP11; SpectrumGreen), and 17 (CEP17; Spectrum Aqua) were purchased from Vysis (Abbott Molecular Inc., Mississauga, Ontario, Canada). Chromosomes 8, 11, and 17 were purposefully selected as many genes implicated in ovarian cancer pathogenesis map to these chromosomes including *MYC* (chromosome 8), *CDK12*, and *ATM* (chromosome 11), *TP53*, *BRCA2*, and *NF1* (chromosome 17) [23, 53, 54]. FISH was performed according to the manufacturer (Vysis) with slight modifications. Briefly, cells were seeded into chamber slides ~24 h prior to fixation with 3:1 methanol: acetic acid and pepsin treatment. Cells were rinsed in PBS prior to incubation within a 1×PBS/ 50mM $MgCl_2$ solution. Samples were transferred to a 1% formaldehyde/1×PBS/50mM $MgCl_2$ and a 1×PBS solution, and subsequently dehydrated using an ethanol series (70%, 90% and 100%). DNA was denatured with 70% formamide/2×SSC buffer at 70˚C for 2 min, dehydrated using an ethanol series (70%, 90% and 100%) and stored at -20˚C. The CEP cocktail was prepared by combining CEP11 and CEP17 with the pre-diluted CEP8, and applied to the cells and incubated overnight in a ThermoBrite slide system at 37˚C. The following day, samples were washed, counterstained with DAPI, mounted in Vectashield anti-fade reagent (Vector Laboratories) and stored at -20˚C until imaged.

Image acquisition

Two-dimensional images were acquired using a Zeiss AxioImager Z2 microscope equipped with a Plan-Neofluar 20x objective (numerical aperture 0.5) and an AxioCam HR charge-coupled device (CCD) camera. Images were collected using DAPI, CFP (SpectrumAqua), FITC (SpectrumGreen) and Cy3 (SpectrumOrange) filter cubes, and a minimum of 180 nuclei/sample was imaged. All images were imported into Imaris v7.7.2 (Bitplane), where image visualization and analyses were performed (see below).

Nuclear area analyses

All images were imported into Imaris where nuclear areas were automatically determined as detailed elsewhere[31]. Briefly, size exclusion filters were employed to eliminate apoptotic bodies and overlapping nuclei, while signal intensity thresholds were applied to remove brightly fluorescing apoptotic bodies and mitotic cells. An edge filter was also applied to remove partial nuclei located along the periphery of each image so that only intact interphase nuclei were analyzed.

CEP analyses

All images were imported into Imaris where the numbers of CEPs within each nucleus were automatically determined as detailed elsewhere[32], but using the same filters/thresholds detailed above (*i.e.* size, signal intensity, and edge). All data were exported into Prism v7 (GraphPad) for statistical analyses (see below) and all figures were generated in Photoshop CS6 (Adobe).

CIN analyses

We previously developed a metric called a CS that describes both the gains and losses of chromosomes (*i.e.* CEP foci) so that quantitative comparisons can be made within and between samples[32]. The CS describes the gains and losses of CEP foci within a given nucleus and can be calculated for each individual CEP (*i.e.* CS_8, CS_{11}, and CS_{17}) or all three CEPs combined (CS_C). A CEP-specific CS value (*e.g.* CS_8) is calculated by the following formula, $[CS_8 = |e_{Chr8} - o_{Chr8}|]$, where the CS equals the absolute value obtained when the observed (*o*) number of CEP8 foci is subtracted from the expected (*e*) number of two CEP8 foci (expect 1 focus/chromosome × 2 chromosomes/cell), while a CS_C value is generated by summing the three CEP-specific CS values (*e.g.* $CS_C = CS_8 + CS_{11} + CS_{17}$). By definition, a $CS_C = 0$ identifies a diploid state for the specific chromosomes under investigation. To generate an overall mCS for a given sample, the individual CS values for all the enumerated nuclei in the sample are summed and divided by the total number of nuclei evaluated (*n*);

$$\text{mCS} = \frac{1}{n}\sum_{i=1}^{n}(|e_8 - o_8| + |e_{11} - o_{11}| + |e_{17} - o_{17}|)_i$$

Statistical analysis

All data were imported into Prism v7 where standard statistics and analyses were generated including mean, standard deviation and Student's *t*-tests. Differences between the cumulative distribution frequencies for nuclear areas and the CS values (combined [CS_C] and individual [CS_8, CS_{11}, or CS_{17}] and combined) were statistically compared using a two-sample KS-test with a confidence interval of 0.05 (α statistic).

Supporting information

S1 Fig. Primary EOC Samples Can Exhibit Extreme Levels of CIN. (A) High resolution image of a nucleus isolated from sample G of EOC16. DNA is counterstained with DAPI (blue), while CEPs 8, 11 and 17 are labeled red, green and yellow, respectively, within the Merge. Presented are the widefield fluorescent images (top) and the corresponding rendered images (bottom). Note the scale bar represents 5 μm and the nucleus is markedly larger than those presented in Fig 1A. The CS_8 (41), CS_{11} (31) and CS_{17} (21) values are included and collectively produce a CS_C value = 93 indicating an extreme level of aneuploidy and CIN within this cell.
(TIF)

S2 Fig. CIN is Dynamic and Changes in Response to Carboplatin/Paclitaxel Treatments. (A) Cumulative distribution frequency graph presenting the nuclear areas arranged smallest to largest for each sample evaluated from EOC73. **(B)** Graph presenting the cumulative distribution frequencies for CS_C values from each sample. **(C)** Cumulative distribution frequency

graphs for CS_8 (left), CS_{11} (middle), and CS_{17} (right).
(TIF)

S3 Fig. Increases in CIN Occur in Recurrent EOC. (A) Graph presenting the cumulative nuclear area distribution frequencies presented from smallest to largest for each sample evaluated from EOC13. **(B)** Graph presenting the cumulative distribution frequencies for CS_C values. **(C)** Cumulative distribution frequency graphs for CS_8 (left), CS_{11} (middle), and CS_{17} (right).
(TIF)

S4 Fig. High Levels of CIN are Associated with Recurrent EOC. (A) Graph depicting the cumulative distribution frequency of all nuclear areas (presented smallest to largest) evaluated in samples collected from EOC140. **(B)** Cumulative distribution frequency graph presenting the CS_C values from each sample. **(C)** Individual cumulative distribution frequency graphs for CS_8 (left), CS_{11} (middle) and CS_{17} (right).
(TIF)

S5 Fig. CIN Increases in Aggressive, Platinum Resistant EOC. (A) Cumulative distribution frequency graph for nuclear areas (presented smallest to largest) evaluated in samples collected from EOC16. **(B)** Cumulative distribution frequency graph presenting the CS_C values from each sample. **(C)** Cumulative frequency distribution graphs presenting the individual CS values from each nucleus quantified within each sample.
(TIF)

S6 Fig. The Levels of CIN Appear Static in PEO1 and PEO4 Cells. (A) Cumulative distribution frequency graph for all nuclear areas measured within PEO1 and PEO4 (presented smallest to largest) indicating the nuclear areas are largely similar in both lines. **(B)** Cumulative distribution frequency graph for CS_C values from PEO1 and PEO4 cells. **(C)** Cumulative distribution frequency graphs for CS_8 (left), CS_{11} (middle) and CS_{17} (right) from PEO1 and PEO4.
(TIF)

S7 Fig. A2780s and A2780cp Cells Exhibit Similar Levels of CIN. (A) Scatter plot (left) depicting the nuclear area distribution for A2780s (sensitive) and A2780cp (resistant) cells with the interquartile ranges (25th, 50th and 75th percentiles) identified in red. Cumulative distribution frequency graph (right) for all nuclear areas measured within A2780s and A2780cp arranged smallest to largest. **(B)** Scatter plot (left) depicting the CS_C distribution for nuclei in A2780s and A2780cp cells. Cumulative CS_C distribution frequency graph (right) from A2780s and A2780cp cells. **(C)** Scatter plots presenting the gains and losses of CEP 8 (CS_8; left), 11 (CS_{11}; middle) and 17 (CS_{17}; right) for each nucleus analyzed in A2780s and A2780cp. **(D)** Cumulative distribution frequency graphs for CS_8 (left), CS_{11} (middle) and CS_{17} (right) from A2780s and A2780cp.
(TIF)

S1 Table. Primary EOC Patient Sample Clinical Details.
[A]optimal surgical debulking ($<$5 mm)
[B]no surgery
[C]total abdominal hysterectomy, bilateral salpingo-oophorectomy, omentectomy (no note on debulking).
(DOCX)

S2 Table. Nuclear Area Statistics for Patient Samples.
[A]Presented in numerical order

[B]Number of nuclei analyzes (N)
[C]Standard deviation (SD)
[D]Fold increase in mean nuclear area relative to the earliest sample collected from a given patient (N/A; not applicable).
(DOCX)

S3 Table. KS-tests Comparing the Cumulative Nuclear Area Distribution Frequencies in EOC18[A].
[A]Presented are the *p*-values calculated from two-sample KS-tests for the indicated pairs with *p*-values <0.05 are considered statistically significant.
(DOCX)

S4 Table. KS-tests Comparing the Cumulative CS Distribution Frequencies in EOC18[A].
[A]Presented are the *p*-values calculated from two-sample KS-tests for the indicated pairs with *p*-values <0.05 are considered statistically significant.
(DOCX)

S5 Table. KS-tests Comparing the Cumulative Nuclear Area Distribution Frequencies in EOC73[A].
[A]Presented are the *p*-values calculated from two-sample KS-tests for the indicated pairs with *p*-values <0.05 considered statistically significant.
(DOCX)

S6 Table. KS-tests Comparing the Cumulative CS Distribution Frequencies in EOC73[A].
[A]Presented are the *p*-values calculated from two-sample KS-tests for the indicated pairs with *p*-values <0.05 considered statistically significant.
(DOCX)

S7 Table. KS-tests Comparing the Cumulative Nuclear Area Distribution Frequencies in EOC13[A].
[A]Presented are the *p*-values calculated from two-sample KS-tests for the indicated pairs with *p*-values <0.05 considered statistically significant.
(DOCX)

S8 Table. KS-tests Comparing the Cumulative Nuclear Area Distribution Frequencies in EOC140[A].
[A]Presented are the *p*-values calculated from two-sample KS-tests for the indicated pairs with *p*-values <0.05 are considered statistically significant.
(DOCX)

S9 Table. KS-tests Comparing the Cumulative CS Distribution Frequencies in EOC13[A].
[A]Presented are the *p*-values calculated from two-sample KS-tests for the indicated pairs with *p*-values <0.05 considered statistically significant.
(DOCX)

S10 Table. KS-tests Comparing the Cumulative Nuclear Area Distribution Frequencies in EOC140[A].
[A]Presented are the *p*-values calculated from two-sample KS-tests for the indicated pairs with *p*-values <0.05 are considered statistically significant.
(DOCX)

S11 Table. KS-tests Comparing the Cumulative Nuclear Area Distribution Frequencies in EOC16[A].

[A]Presented are the *p*-values calculated from two-sample KS-tests for the indicated pairs with *p*-values <0.05 considered statistically significant.
(DOCX)

S12 Table. KS-tests Comparing the Cumulative CS Distribution Frequencies in EOC16[A].
[A]Presented are the *p*-values calculated from two-sample KS-tests for the indicated pairs with *p*-values <0.05 considered statistically significant.
(DOCX)

S13 Table. Nuclear Area Statistics for PEO1/4 and A2780s/cp Cells.
[A]Number of nuclei analyzes (N)
[B]Standard deviation (SD)
[C]Fold increase in mean nuclear area.
(DOCX)

Acknowledgments

Author Contributions

Conceptualization: MWN KJM.

Formal analysis: SPG MN MWN KJM.

Investigation: SPG MN ZL JLA.

Resources: ADA.

Writing – original draft: SPG MWN KJM.

Writing – review & editing: SPG ADA MWN KJM.

References

1. Ferlay J SI, Ervik M, Dikshit R, Eser S, Mathers C, Rebelo M, Parkin DM, Forman D, Bray, F. GLOBO-CAN 2012 v1.1, Cancer Incidence and Mortality Worldwide: IARC CancerBase No. 11 Lyon, France2014 [04/12/2015]. Available from: http://globocan.iarc.fr/.

2. Kobel M, Bak J, Bertelsen BI, Carpen O, Grove A, Hansen ES, et al. Ovarian carcinoma histotype determination is highly reproducible, and is improved through the use of immunohistochemistry. Histopathology. 2014; 64(7):1004–13. https://doi.org/10.1111/his.12349 PMID: 24329781

3. Sherman-Baust CA, Becker KG, Wood Iii WH, Zhang Y, Morin PJ. Gene expression and pathway analysis of ovarian cancer cells selected for resistance to cisplatin, paclitaxel, or doxorubicin. Journal of ovarian research. 2011; 4(1):21. PubMed Central PMCID: PMC3259089. https://doi.org/10.1186/1757-2215-4-21 PMID: 22141344

4. Hiss D. Optimizing molecular-targeted therapies in ovarian cancer: the renewed surge of interest in ovarian cancer biomarkers and cell signaling pathways. Journal of oncology. 2012; 2012:737981. PubMed Central PMCID: PMC3306947. https://doi.org/10.1155/2012/737981 PMID: 22481932

5. Coleman RL, Monk BJ, Sood AK, Herzog TJ. Latest research and treatment of advanced-stage epithelial ovarian cancer. Nature reviews Clinical oncology. 2013; 10(4):211–24. PubMed Central PMCID: PMC3786558. https://doi.org/10.1038/nrclinonc.2013.5 PMID: 23381004

6. Pujade-Lauraine E, Hilpert F, Weber B, Reuss A, Poveda A, Kristensen G, et al. Bevacizumab combined with chemotherapy for platinum-resistant recurrent ovarian cancer: The AURELIA open-label

randomized phase III trial. J Clin Oncol. 2014; 32(13):1302–8. https://doi.org/10.1200/JCO.2013.51. 4489 PMID: 24637997

7. Bowtell DD, Bohm S, Ahmed AA, Aspuria PJ, Bast RC Jr., Beral V, et al. Rethinking ovarian cancer II: reducing mortality from high-grade serous ovarian cancer. Nature reviews Cancer. 2015; 15(11):668– 79. PubMed Central PMCID: PMC4892184. https://doi.org/10.1038/nrc4019 PMID: 26493647

8. Lengauer C, Kinzler KW, Vogelstein B. Genetic instability in colorectal cancers. Nature. 1997; 386 (6625):623–7. https://doi.org/10.1038/386623a0 PMID: 9121588

9. Lengauer C, Kinzler KW, Vogelstein B. Genetic instabilities in human cancers. Nature. 1998; 396 (6712):643–9. https://doi.org/10.1038/25292 PMID: 9872311

10. Pikor L, Thu K, Vucic E, Lam W. The detection and implication of genome instability in cancer. Cancer Metastasis Rev. 2013; 32(3–4):341–52. PubMed Central PMCID: PMCPMC3843371. https://doi.org/ 10.1007/s10555-013-9429-5 PMID: 23633034

11. Geigl JB, Obenauf AC, Schwarzbraun T, Speicher MR. Defining 'chromosomal instability'. Trends Genet. 2008; 24(2):64–9. https://doi.org/10.1016/j.tig.2007.11.006 PMID: 18192061

12. Cosenza MR, Kramer A. Centrosome amplification, chromosomal instability and cancer: mechanistic, clinical and therapeutic issues. Chromosome research: an international journal on the molecular, supra-molecular and evolutionary aspects of chromosome biology. 2016; 24(1):105–26.

13. Thompson SL, Bakhoum SF, Compton DA. Mechanisms of chromosomal instability. Current biology: CB. 2010; 20(6):R285–95. PubMed Central PMCID: PMC3781365. https://doi.org/10.1016/j.cub.2010. 01.034 PMID: 20334839

14. Carter SL, Eklund AC, Kohane IS, Harris LN, Szallasi Z. A signature of chromosomal instability inferred from gene expression profiles predicts clinical outcome in multiple human cancers. Nature genetics. 2006; 38(9):1043–8. https://doi.org/10.1038/ng1861 PMID: 16921376

15. Duesberg P, Stindl R, Hehlmann R. Explaining the high mutation rates of cancer cells to drug and multi-drug resistance by chromosome reassortments that are catalyzed by aneuploidy. Proceedings of the National Academy of Sciences of the United States of America. 2000; 97(26):14295–300. PubMed Central PMCID: PMC18912. https://doi.org/10.1073/pnas.97.26.14295 PMID: 11121035

16. Duesberg P, Stindl R, Hehlmann R. Origin of multidrug resistance in cells with and without multidrug resistance genes: chromosome reassortments catalyzed by aneuploidy. Proceedings of the National Academy of Sciences of the United States of America. 2001; 98(20):11283–8. PubMed Central PMCID: PMC58721. https://doi.org/10.1073/pnas.201398998 PMID: 11553793

17. Fabarius A, Hehlmann R, Duesberg PH. Instability of chromosome structure in cancer cells increases exponentially with degrees of aneuploidy. Cancer Genet Cytogenet. 2003; 143(1):59–72. Epub 2003/ 05/14. PMID: 12742157

18. Lee AJ, Endesfelder D, Rowan AJ, Walther A, Birkbak NJ, Futreal PA, et al. Chromosomal instability confers intrinsic multidrug resistance. Cancer research. 2011; 71(5):1858–70. PubMed Central PMCID: PMC3059493. https://doi.org/10.1158/0008-5472.CAN-10-3604 PMID: 21363922

19. Swanton C, Nicke B, Schuett M, Eklund AC, Ng C, Li Q, et al. Chromosomal instability determines tax-ane response. Proceedings of the National Academy of Sciences of the United States of America. 2009; 106(21):8671–6. PubMed Central PMCID: PMC2688979. https://doi.org/10.1073/pnas. 0811835106 PMID: 19458043

20. Baumbusch LO, Helland A, Wang Y, Liestol K, Schaner ME, Holm R, et al. High levels of genomic aber-rations in serous ovarian cancers are associated with better survival. PloS one. 2013; 8(1):e54356. PubMed Central PMCID: PMC3553118. https://doi.org/10.1371/journal.pone.0054356 PMID: 23372714

21. Bayani J, Brenton JD, Macgregor PF, Beheshti B, Albert M, Nallainathan D, et al. Parallel analysis of sporadic primary ovarian carcinomas by spectral karyotyping, comparative genomic hybridization, and expression microarrays. Cancer research. 2002; 62(12):3466–76. PMID: 12067990

22. Bayani J, Paderova J, Murphy J, Rosen B, Zielenska M, Squire JA. Distinct patterns of structural and numerical chromosomal instability characterize sporadic ovarian cancer. Neoplasia. 2008; 10 (10):1057–65. PubMed Central PMCID: PMC2546587. PMID: 18813350

23. Cancer Genome Atlas Research Network. Integrated genomic analyses of ovarian carcinoma. Nature. 2011; 474(7353):609–15. PubMed Central PMCID: PMC3163504. https://doi.org/10.1038/nature10166 PMID: 21720365

24. Cooke SL, Ng CK, Melnyk N, Garcia MJ, Hardcastle T, Temple J, et al. Genomic analysis of genetic het-erogeneity and evolution in high-grade serous ovarian carcinoma. Oncogene. 2010; 29(35):4905–13. PubMed Central PMCID: PMCPMC2933510. https://doi.org/10.1038/onc.2010.245 PMID: 20581869

25. Etemadmoghadam D, deFazio A, Beroukhim R, Mermel C, George J, Getz G, et al. Integrated genome-wide DNA copy number and expression analysis identifies distinct mechanisms of primary

chemoresistance in ovarian carcinomas. Clin Cancer Res. 2009; 15(4):1417–27. PubMed Central PMCID: PMCPMC2670486. https://doi.org/10.1158/1078-0432.CCR-08-1564 PMID: 19193619

26. George J, Alsop K, Etemadmoghadam D, Hondow H, Mikeska T, Dobrovic A, et al. Nonequivalent gene expression and copy number alterations in high-grade serous ovarian cancers with BRCA1 and BRCA2 mutations. Clin Cancer Res. 2013; 19(13):3474–84. https://doi.org/10.1158/1078-0432.CCR-13-0066 PMID: 23633455

27. Gorringe KL, Jacobs S, Thompson ER, Sridhar A, Qiu W, Choong DY, et al. High-resolution single nucleotide polymorphism array analysis of epithelial ovarian cancer reveals numerous microdeletions and amplifications. Clin Cancer Res. 2007; 13(16):4731–9. https://doi.org/10.1158/1078-0432.CCR-07-0502 PMID: 17699850

28. Patch AM, Christie EL, Etemadmoghadam D, Garsed DW, George J, Fereday S, et al. Whole-genome characterization of chemoresistant ovarian cancer. Nature. 2015; 521(7553):489–94. https://doi.org/10.1038/nature14410 PMID: 26017449

29. Wang ZC, Birkbak NJ, Culhane AC, Drapkin R, Fatima A, Tian R, et al. Profiles of genomic instability in high-grade serous ovarian cancer predict treatment outcome. Clin Cancer Res. 2012; 18(20):5806–15. PubMed Central PMCID: PMCPMC4205235. https://doi.org/10.1158/1078-0432.CCR-12-0857 PMID: 22912389

30. Ciriello G, Miller ML, Aksoy BA, Senbabaoglu Y, Schultz N, Sander C. Emerging landscape of onco-genic signatures across human cancers. Nature genetics. 2013; 45(10):1127–33. PubMed Central PMCID: PMCPMC4320046. https://doi.org/10.1038/ng.2762 PMID: 24071851

31. Thompson LL, McManus KJ. A novel multiplexed, image-based approach to detect phenotypes that underlie chromosome instability in human cells. PloS one. 2015; 10(4):e0123200. PubMed Central PMCID: PMC4404342. https://doi.org/10.1371/journal.pone.0123200 PMID: 25893404

32. Cisyk AL, Penner-Goeke S, Lichtensztejn Z, Nugent Z, Wightman RH, Singh H, et al. Characterizing the prevalence of chromosome instability in interval colorectal cancer. Neoplasia. 2015; 17(3):306–16. PubMed Central PMCID: PMC4372653. https://doi.org/10.1016/j.neo.2015.02.001 PMID: 25810015

33. Lengyel E. Ovarian cancer development and metastasis. The American journal of pathology. 2010; 177 (3):1053–64. PubMed Central PMCID: PMC2928939. https://doi.org/10.2353/ajpath.2010.100105 PMID: 20651229

34. Ahmed N, Stenvers KL. Getting to know ovarian cancer ascites: opportunities for targeted therapy-based translational research. Frontiers in oncology. 2013; 3:256. PubMed Central PMCID: PMC3782691. https://doi.org/10.3389/fonc.2013.00256 PMID: 24093089

35. Wolf CR, Hayward IP, Lawrie SS, Buckton K, McIntyre MA, Adams DJ, et al. Cellular heterogeneity and drug resistance in two ovarian adenocarcinoma cell lines derived from a single patient. International journal of cancer. 1987; 39(6):695–702. PMID: 3583449

36. Behrens BC, Hamilton TC, Masuda H, Grotzinger KR, Whang-Peng J, Louie KG, et al. Characterization of a cis-diamminedichloroplatinum(II)-resistant human ovarian cancer cell line and its use in evaluation of platinum analogues. Cancer research. 1987; 47(2):414–8. PMID: 3539322

37. Langdon SP, Lawrie SS, Hay FG, Hawkes MM, McDonald A, Hayward IP, et al. Characterization and properties of nine human ovarian adenocarcinoma cell lines. Cancer research. 1988; 48(21):6166–72. PMID: 3167863

38. Ince TA, Sousa AD, Jones MA, Harrell JC, Agoston ES, Krohn M, et al. Characterization of twenty-five ovarian tumour cell lines that phenocopy primary tumours. Nat Commun. 2015; 6:7419. PubMed Central PMCID: PMCPMC4473807. https://doi.org/10.1038/ncomms8419 PMID: 26080861

39. Dent J, Hall GD, Wilkinson N, Perren TJ, Richmond I, Markham AF, et al. Cytogenetic alterations in ovarian clear cell carcinoma detected by comparative genomic hybridisation. British journal of cancer. 2003; 88(10):1578–83. PubMed Central PMCID: PMC2377123. https://doi.org/10.1038/sj.bjc.6600896 PMID: 12771925

40. Evans MF, McDicken IW, Herrington CS. Numerical abnormalities of chromosomes 1, 11, 17, and X are associated with stromal invasion in serous and mucinous epithelial ovarian tumours. The Journal of pathology. 1999; 189(1):53–9. https://doi.org/10.1002/(SICI)1096-9896(199909)189:1<53::AID-PATH393>3.0.CO;2-U PMID: 10451488

41. Israeli O, Gotlieb WH, Friedman E, Korach J, Friedman E, Goldman B, et al. Genomic analyses of primary and metastatic serous epithelial ovarian cancer. Cancer Genet Cytogenet. 2004; 154(1):16–21. https://doi.org/10.1016/j.cancergencyto.2004.02.006 PMID: 15381367

42. Lin YS, Eng HL, Jan YJ, Lee HS, Ho WL, Liou CP, et al. Molecular cytogenetics of ovarian granulosa cell tumors by comparative genomic hybridization. Gynecologic oncology. 2005; 97(1):68–73. https://doi.org/10.1016/j.ygyno.2004.12.014 PMID: 15790439

43. Pejovic T, Yates JE, Liu HY, Hays LE, Akkari Y, Torimaru Y, et al. Cytogenetic instability in ovarian epithelial cells from women at risk of ovarian cancer. Cancer research. 2006; 66(18):9017–25. https://doi.org/10.1158/0008-5472.CAN-06-0222 PMID: 16982743

44. Rotmensch J, Turkula TE, Weichselbaum RR, Schwartz JL. Cytogenetic observations of a human ovarian carcinoma clinically resistant to therapy. American journal of obstetrics and gynecology. 1988; 159 (5):1099–103. PMID: 3189443

45. Taetle R, Aickin M, Yang JM, Panda L, Emerson J, Roe D, et al. Chromosome abnormalities in ovarian adenocarcinoma: I. Nonrandom chromosome abnormalities from 244 cases. Genes, chromosomes & cancer. 1999; 25(3):290–300.

46. Thompson FH, Liu Y, Emerson J, Weinstein R, Makar R, Trent JM, et al. Simple numeric abnormalities as primary karyotype changes in ovarian carcinoma. Genes, chromosomes & cancer. 1994; 10(4):262–6.

47. Wasenius VM, Jekunen A, Monni O, Joensuu H, Aebi S, Howell SB, et al. Comparative genomic hybridization analysis of chromosomal changes occurring during development of acquired resistance to cisplatin in human ovarian carcinoma cells. Genes, chromosomes & cancer. 1997; 18(4):286–91.

48. Zeimet AG, Fiegl H, Goebel G, Kopp F, Allasia C, Reimer D, et al. DNA ploidy, nuclear size, proliferation index and DNA-hypomethylation in ovarian cancer. Gynecologic oncology. 2011; 121(1):24–31. PubMed Central PMCID: PMC3062717. https://doi.org/10.1016/j.ygyno.2010.12.332 PMID: 21251700

49. Teyssier JR, Benard J, Ferre D, Da Silva J, Renaud L. Drug-related chromosomal changes in chemoresistant human ovarian carcinoma cells. Cancer Genet Cytogenet. 1989; 39(1):35–43. PMID: 2731146

50. Birkbak NJ, Eklund AC, Li Q, McClelland SE, Endesfelder D, Tan P, et al. Paradoxical relationship between chromosomal instability and survival outcome in cancer. Cancer research. 2011; 71 (10):3447–52. PubMed Central PMCID: PMCPMC3096721. https://doi.org/10.1158/0008-5472.CAN-10-3667 PMID: 21270108

51. Roylance R, Endesfelder D, Gorman P, Burrell RA, Sander J, Tomlinson I, et al. Relationship of extreme chromosomal instability with long-term survival in a retrospective analysis of primary breast cancer. Cancer Epidemiol Biomarkers Prev. 2011; 20(10):2183–94. PubMed Central PMCID: PMCPMC3199437. https://doi.org/10.1158/1055-9965.EPI-11-0343 PMID: 21784954

52. Theriault BL, Portelance L, Mes-Masson AM, Nachtigal MW. Establishment of primary cultures from ovarian tumor tissue and ascites fluid. Methods in molecular biology. 2013; 1049:323–36. https://doi.org/10.1007/978-1-62703-547-7_24 PMID: 23913227

53. Chen CH, Shen J, Lee WJ, Chow SN. Overexpression of cyclin D1 and c-Myc gene products in human primary epithelial ovarian cancer. International journal of gynecological cancer: official journal of the International Gynecological Cancer Society. 2005; 15(5):878–83.

54. Thorstenson YR, Roxas A, Kroiss R, Jenkins MA, Yu KM, Bachrich T, et al. Contributions of ATM mutations to familial breast and ovarian cancer. Cancer research. 2003; 63(12):3325–33. PMID: 12810666